Chapter 4

Semi-infinite Moving Crack under Antiplane Shear Loading

4.1 Introduction

Cracks in materials are always a primary concern for engineers and scientists in designing a mechanical structure. The development of cracks in materials is widespread, mainly when the material consists of various layers or strips, to increase the durability of the material , which goes through numerous disturbances by the outer environment that can cause the cracks to propagate. The cracks on the surface and at the interface are prevalent when those tend to propagate with a higher propagation rate, which can lead to one of the causes of structural failures by creating a fracture in the material. Stress intensity factor(SIF) and Crack opening displacement(COD) are physical quatities which are determined to study the behaviour of crack propagation in the mechnical structures.

Composite materials are high in demand due to their durability, light weight, resistence for high pressure and wide range of applications. These materials are well known for their unique mechanical properties in three orthogonal directions. A bunch of different types of cracks can occure in composite materials in which moving semi-infinite interfacial cracks under anti-plane shear stress are one of a kind. Interfacial anti-plane shear cracks are very likely to occure in fiber inforced composite materials as the interface usually develop the nucleus of crack propagation and fracture initiation.

Anti-plane shear stress occurs at the crack tips when the body is deformed in such a way that only a non-vanishing factor is found in the Anti-plane direction.

The cracks under anti-plane shear loading have been studied by many researchers till date, because of the nature of sudden crack occurrence under the shear loading. The concept of anti-plane shear stress has been described enormously by Sih and Chen [104]. The moving interfacial Griffith crack in dissimilar orthotropic has been studied by Das and Patra [51]. Nanoscale mode-III interfacial crack in bimaterial has been studied by Yang et at. [105] and the effect of thickness on the crack propagation for antiplane crack mode has been examined and studied by Bidadi et al. [106]. The concept of moving crack has been first given by Yoffee [36]. Semi-infinite crack situated in orthotropic strip with clamped boundaries has been studied by Georgiadis and Papadopoulos [107]. Interaction between anti-plane semi-infinite crack and a screw dislocation [108] and semi-infinite mode-III crack penetration [109] have been studies by Wang and Schiavona.

The disturbance created by SH waves on the crack surfaces has always been fascinating for researchers, due to its various effects on the crack propagation. A large number of studies have been conducted on the nature of waves in course of fracture mechanics. The scattering effect of plane SH waves has been investigated by Trifunac [110] and the steady-state SH waves effect in a bi-material half space has been studied by Yang and Qi [111]. An interfacial linear crack interacting by a circular cavity has been been solved by Diankui [112].

In dynamic fracture mechanics, several crack propagation problems in a strip in complex transform plane can be reduced to Wiener-Hopf equation. The method of Wiener-Hopf Technique used in the present chapter is initially given by B. Noble in his book [113], which was further studied by many researchers and engineers. In this technique, factorization of the kernel is most difficult step. The method to find asymptotic expression of SIF without the visible factorization of the kernel in the Wiener-Hopf technique has been given by Nilsson [114] [115]. Elastodynamic stress intensity factor for semi-infinite crack has been studied by Achenbach and Gautesen [39]. Some problems consist of different types of cracks in dymnamic elasticity using Wierner-Hopf technique have been investigated by Abrahams [116]. The model consists of two semi- infinite cracks on square lattice has been solved by Maurya and Sharma [117]. Therefore, it is found from the literature survey that most of the works related to the semi-infinite cracks are embedded type. The investigation of SIF and COD for a moving interfacial semi-infinite crack with SH-waves disturbance and antiplane shear loading for dissimilar orthotropic strips in this chapter, is first of its kind.

In this chapter, a moving semi-infinite mode-III crack under antiplane shear loading is considered at the interface of two semi-infinite orthotropic strips of the same depth h. Both the strips are of different composite materials. The semi-infinite crack is moving with constant crack velocity (V) at the interface of the orthotropic strips. The problem has been solved by using the Wiener-Hopf technique along with the Fourier transform. The expressions of the SIF and COD have been derived analytically. The numerical simulation results of the said physical quantities have been depicted graphically for the combinations of different material values of the strips, depths of the strips and crack velocities.

4.2 Mathematical formulation of the problem

Let us consider a semi-infinite moving crack situated at the interface of two semi-infinite orthotropic strips. Also, consider that $(X < Y < Z)$ is the fixed cartesian coordinate that coincides with the origin of the moving crack system so that the crack position is $(-\infty < X < 0, Y = 0)$ as shown in. Let the crack is propagating with a constant velocity V in the positive direction of X-axis. At any time t, the position of the crack is $-\infty < X < Vt$, $Y = 0$. The crack is under antiplane shear loading. Therefore, the displacement component is found only out of the plane direction, i.e., in Z-direction only, given as $W^{(j)} = W^{(j)}(X, Y, t)$.

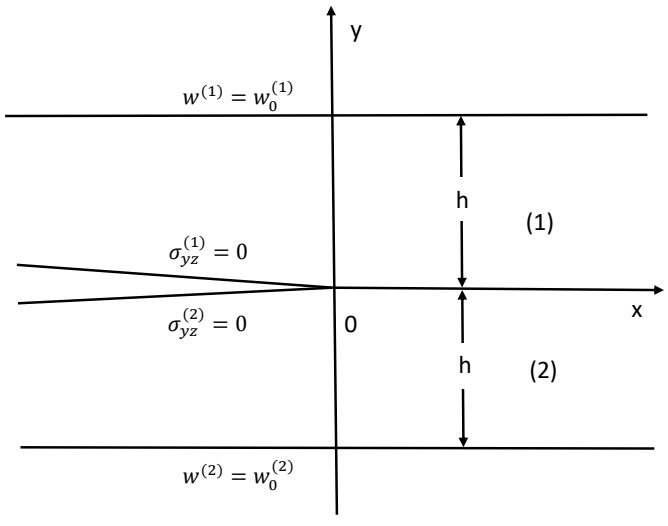

Figure 4.1: Geometry of the main problem

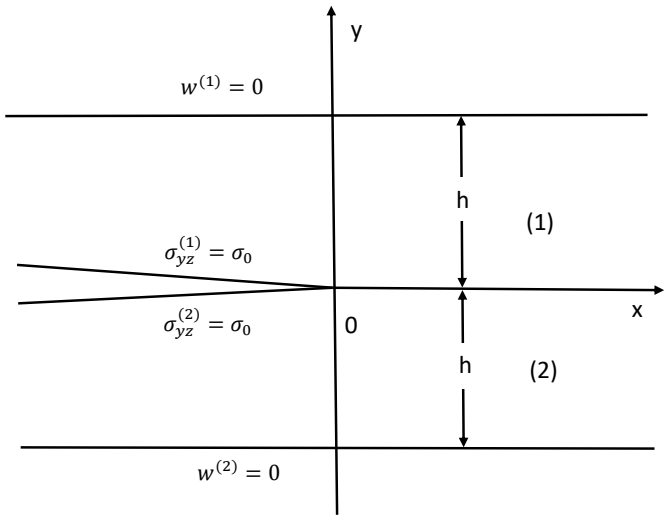

Figure 4.2: Geometry of the transformed problem

The relation between shear stress and displacement component for the model is given by

$$\sigma_{XZ}^{(j)} = C_{55}^{(j)} \frac{\partial W^{(j)}}{\partial X},$$

$$\sigma_{YZ}^{(j)} = C_{44}^{(j)} \frac{\partial W^{(j)}}{\partial Y}, \tag{4.2.1}$$

where $C_{44}^{(j)}$'s and $C_{55}^{(j)}$'s are the principal shear moduli in X and Y directions, respectively for different orthotropic materials. Here, $j = 1$ for semi-infinite strip-1 as medium-I and $j = 2$ for semi-infinite strip-2 as medium-II. The antiplane equation of motion is given by

$$C_{55}^{(j)} \frac{\partial^2 W^{(j)}}{\partial X^2} + C_{44}^{(j)} \frac{\partial^2 W^{(j)}}{\partial Y^2} = \rho^{(j)} \frac{\partial^2 W^{(j)}}{\partial t^2}, \tag{4.2.2}$$

where $\rho^{(j)}$'s are the material densities.

Let us rewrite the Eq.(4.2.2) as

$$\frac{\partial^2 W^{(j)}}{\partial X^2} + \beta^{(j)} \frac{\partial^2 W^{(j)}}{\partial Y^2} = \frac{1}{C_s^{(j)}} \frac{\partial^2 W^{(j)}}{\partial t^2}, \tag{4.2.3}$$

where $\beta^{(j)} = \frac{C_{44}^{(j)}}{C_{55}^{(j)}}$ and $C_s^{(j)}$'s are the SH-wave velocity of the orthotropic materials given as $C_s^{(j)} = \sqrt{\frac{C_{55}^{(j)}}{\rho^{(j)}}}$.

Now, applying the Galilean transformation as $x = X - Vt, y = Y$ and $t = t$ on the Eq.(4.2.3) to make the model free from time t, given as

$$G^{(j)2}\frac{\partial^2 w^{(j)}}{\partial x^2}+\frac{\partial^2 w^{(j)}}{\partial y^2}=0, \tag{4.2.4}$$

where $G^{(j)2}=\frac{1}{\beta^{(j)2}}(1-\frac{V^2}{C_s^{(j)2}})$ and $w^{(j)}(x,y)=W^{(j)}(X,Y,t)$ are the displacement components in antiplane direction.

The boundary and continuity conditions for the given problem as shown in Fig.4.1, are considered as

$$\sigma_{yz}^{(1)}(x,0+)=\sigma_{yz}^{(2)}(x,0-)=0, \qquad x<0, \tag{4.2.5}$$
$$w^{(1)}(x,0)=w^{(2)}(x,0), \qquad x>0, \tag{4.2.6}$$
$$\sigma_{yz}^{(1)}(x,0)=\sigma_{yz}^{(2)}(x,0), \qquad x>0, \tag{4.2.7}$$
$$w^{(j)}(x,\pm h)=w_0^{(j)}, \qquad -\infty<x<\infty, \tag{4.2.8}$$
$$\sigma_{yz}^{(j)}(x,\pm h)=0, \qquad -\infty<x<\infty, \tag{4.2.9}$$

where $w_0^{(j)}$'s $(j=1,2)$ are the displacement constants. In order to apply the Wiener-Hopf Technique, the above set of conditions should be changed slightly by superimposing a constant load σ_0 on the crack surface. Now the boundary conditions as shown in Fig. 4.2, become

$$\sigma_{yz}^{(1)}(x,0+)=\sigma_{yz}^{(2)}(x,0-)=\sigma_0, \qquad x<0, \tag{4.2.10}$$
$$w^{(1)}(x,0)=w^{(2)}(x,0), \qquad x>0, \tag{4.2.11}$$
$$\sigma_{yz}^{(1)}(x,0)=\sigma_{yz}^{(2)}(x,0), \qquad x>0, \tag{4.2.12}$$
$$w^{(1)}(x,h)=0, \qquad -\infty<x<\infty, \tag{4.2.13}$$
$$w^{(2)}(x,-h)=0, \qquad -\infty<x<\infty, \tag{4.2.14}$$
$$\sigma_{yz}^{(1)}(x,h)=0, \qquad -\infty<x<\infty, \tag{4.2.15}$$
$$\sigma_{yz}^{(2)}(x,-h)=0, \qquad -\infty<x<\infty. \tag{4.2.16}$$

The values of $w_0^{(j)}$'s are to be choosen in such a way that the shear loading on the crack surface is equal and given by the following relation

$$C_{44}^{(1)}w_0^{(1)}=C_{44}^{(2)}w_0^{(2)}. \tag{4.2.17}$$

Also the above defined two sets of boundary conditions refere to the same problem for a particular value of σ_0 as per Georgiadis [107], given by

$$\sigma_0 = \frac{-C_{44}^{(1)} w_0^{(1)}}{h} = \frac{-C_{44}^{(2)} w_0^{(2)}}{h}. \tag{4.2.18}$$

Now the boundary condition (4.2.10) can be modified as

$$\sigma_{yz}^{(1)}(x, 0+) = \sigma_0 e^{\epsilon x}, \qquad x < 0, \tag{4.2.19}$$

where ϵ is a very small positive quatity, which is tending to zero.

Fourier transformation on the boundary conditions, we get

$$\overline{\sigma}_{yz}^{(1)}(x, 0) = \overline{\sigma}_{yz}^{(2)}(x, 0), \tag{4.2.20}$$
$$\overline{w}^{(1)}(x, 0) = \overline{w}^{(2)}(x, 0), \tag{4.2.21}$$
$$\overline{w}^{(1)}(x, h) = 0, \tag{4.2.22}$$
$$\overline{w}^{(2)}(x, -h) = 0. \tag{4.2.23}$$

The solution of the Eq.(4.2.4) can be assumed as

$$\overline{w}^{(j)}(\xi, y) = P^{(j)}(\xi) e^{-G^{(j)}\xi y} + Q^{(j)}(\xi) e^{G^{(j)}\xi y}, \tag{4.2.24}$$

where $P^{(j)}$'s and $Q^{(j)}$'s are the unknown coefficients to be determined. The antiplane shear stress components are given by

$$\overline{\sigma}_{yz}^{(1)}(\xi, y) = -C_{44}^{(j)} G^{(j)} \xi \left(P^{(j)}(\xi) e^{-G^{(j)}\xi y} - Q^{(j)}(\xi) e^{G^{(j)}\xi y} \right). \tag{4.2.25}$$

4.3 Solution of the problem

Let us consider two unknown funcions given as

$$\sigma_{yz}^{(1)}(x, 0) = m(x), \qquad x > 0, \tag{4.3.1}$$
$$w^{(1)}(x, 0) - w^{(2)}(x, 0) = n(x), \quad x < 0, \tag{4.3.2}$$

with the transformations as

$$\overline{m}_+(\xi) = \frac{1}{\sqrt{2\pi}} \int_0^\infty m(x) e^{i\xi x} dx, \tag{4.3.3}$$

$$\overline{n}_-(\xi) = \frac{1}{\sqrt{2\pi}} \int_{-\infty}^0 n(x) e^{i\xi x} dx, \tag{4.3.4}$$

where subscript (+) and (-) denote the analyticity of the functions for some $\lambda \geq 0$ in upper half and $\lambda \leq 0$ in lower half plane, respectively. The functions $\overline{m}_+(\xi)$ and $\overline{n}_-(\xi)$ are bounded at infinity according to the physical behaviour of the problem. Hence, the bounds of the above functions are assumed as

$$| \overline{m}_+(\xi) | < M x^{-l_m}, \quad as\ x \to \infty$$

$$| \overline{n}_-(\xi) | < N | x |^{-l_n}, \quad as\ x \to -\infty$$

for some $l_m > 0$, $l_n > 0$ with M and N are being positive finite numbers. In order to find the unknown coefficients $Q^{(1)}(\xi)$, $P^{(2)}(\xi)$ and $Q^{(2)}(\xi)$ in terms of $P^{(1)}(\xi)$, we use the boundary condtions (4.2.20)-(4.2.23) as

$$Q^{(1)}(\xi) = -e^{-2G^{(1)}\xi h} P^{(1)}(\xi), \tag{4.3.5}$$

$$P^{(2)}(\xi) = \frac{C_{44}^{(1)} G^{(1)} (1 + e^{-2G^{(1)}\xi h})}{C_{44}^{(2)} G^{(2)} (1 + e^{2G^{(2)}\xi h})} P^{(1)}(\xi) = p P^{(1)}(\xi), \tag{4.3.6}$$

$$Q^{(2)}(\xi) = \frac{-C_{44}^{(1)} G^{(1)} (1 + e^{-2G^{(1)}\xi h})}{C_{44}^{(2)} G^{(2)} (1 + e^{-2G^{(2)}\xi h})} P^{(1)}(\xi) = -p e^{2G^{(2)}\xi h} P^{(1)}(\xi), \tag{4.3.7}$$

$$p = \frac{C_{44}^{(1)} G^{(1)} (1 + e^{-2G^{(1)}\xi h})}{C_{44}^{(2)} G^{(2)} (1 + e^{2G^{(2)}\xi h})}. \tag{4.3.8}$$

4.3.1 Wiener-Hopf technique

Using the boundary conditions (4.2.19) and (4.2.11) with the help of Eqs.(4.3.1)-(4.3.4), we get the following pair of equations as

$$\overline{\sigma}_{yz}^{(1)}(\xi,0) = \overline{m}_{+}(\xi) + \frac{\sigma_0}{\sqrt{2\pi}(\epsilon + i\xi)}, \tag{4.3.9}$$

$$\overline{w}^{(1)}(\xi,0) - \overline{w}^{(2)}(\xi,0) = \overline{n}_{-}(\xi). \tag{4.3.10}$$

After some mathematical computations using above Eqs.(4.3.9)-(4.3.10) with the aid of Eqs.(4.3.5)-(4.3.7), we get the following Weiner-Hopf equation in terms of unknown functions $\overline{m}_{+}(\xi)$ and $\overline{n}_{-}(\xi)$ as

$$\overline{m}_{+}(\xi) = K(\xi)\overline{n}_{-}(\xi) - \frac{\sigma_0}{\sqrt{2\pi}(\epsilon + i\xi)}, \tag{4.3.11}$$

where $K(\xi)$ is given by

$$K(\xi) = \frac{-C_{44}^{(1)}G^{(1)}(1 + e^{-2G^{(1)}\xi h})}{(1 - e^{-2G^{(1)}\xi h} - p(1 - e^{2G^{(2)}\xi h}))}. \tag{4.3.12}$$

To find the solution of Eq.(4.3.11), we need to factorize the kernel $K(\xi)$ into the following form as per given by Noble [113]

$$K(\xi) = K_{+}(\xi)K_{-}(\xi), \tag{4.3.13}$$

where the functions $K_{+}(\xi)$ and $K_{-}(\xi)$ are non-zero analytic for $\lambda > \lambda_1(\lambda_1 < 0)$ and $\lambda < \lambda_2(\lambda_2 > 0)$, respectively. Hence, Eq.(4.3.11) with the help of Eq.(4.3.13) becomes

$$\frac{\overline{m}_{+}(\xi)}{K_{+}(\xi)} = K_{-}(\xi)\overline{n}_{-}(\xi) - \frac{\sigma_0}{\sqrt{2\pi}(\epsilon + i\xi)K_{+}(\xi)}. \tag{4.3.14}$$

Now, the last term of the Eq.(4.3.14) can be decomposed in the following manner

$$\frac{\sigma_0}{\sqrt{2\pi}(\epsilon + i\xi)K_{+}(\xi)} = L_{+}(\xi) + L_{-}(\xi), \tag{4.3.15}$$

where

$$L_{+}(\xi) = \frac{\sigma_0}{\sqrt{2\pi}(\epsilon + i\xi)}\left[\frac{1}{K_{+}(\xi)} - \frac{1}{K_{+}(i\epsilon)}\right], \tag{4.3.16}$$

$$L_{-}(\xi) = \frac{\sigma_0}{\sqrt{2\pi}(\epsilon + i\xi)K_{+}(i\epsilon)}. \tag{4.3.17}$$

The functions $L_+(\xi)$ and $L_-(\xi)$ are non-zero analytic in $\lambda > \lambda_1$ and $\lambda < \delta\,(\delta > 0)$, respectively. Rewritting the Eq.(4.3.14) with the help of Eq.(4.3.15), we get

$$\frac{\overline{m}_+(\xi)}{K_+(\xi)} + L_+(\xi) = K_-(\xi)\overline{n}_-(\xi) - L_-(\xi). \tag{4.3.18}$$

In the above Eq.(4.3.18) the functions $\overline{m}_+(\xi), K_+(\xi), L_+(\xi), \overline{n}_-(\xi), K_-(\xi)$ and $L_-(\xi)$ are analytic in the region for $\lambda \geq 0$, $\lambda > \lambda_1(\lambda_1 < 0)$, $\lambda > \lambda_1(\lambda_1 < 0)$, $\lambda \leq 0$, $\lambda < \lambda_2(\lambda_2 > 0)$ and $\lambda < \delta(\delta > 0)$, respectively. Hence, on the left-hand side of the Eq.(4.3.18) is analytic in the upper half-plane ($\lambda \geq 0$), and the right-hand side is analytic in the lower half-plane ($\lambda \leq 0$). Thus, the common area of analyticity is the line $\lambda = 0$. By using the analytic continuation, it is observed that Eq. (4.3.18) is a single-valued analytic function in the whole complex ξ-plane. For the large value of ξ, the functions $K_+(\xi)$ and $K_-(\xi)$ tend to $\xi^{1/2}$ and the functions $\overline{m}_+(\xi)$ and $\overline{n}_-(\xi)$ will be bounded. Let us consider that the both sides of Eq.(4.3.18) equal to an analytic function $A(\xi)$. The LHS of the Eq.(4.3.18) tends to $\xi^{-1/2}$ in the upper half-plane($\lambda \geq 0$) while the RHS tends to $\xi^{1/2}$, for the large value of ξ. Now, by using the extended Liouville theorem, the only analytic function which satisfies both the conditions above is none other than an identically zero function. Therefore, we get

$$A(\xi) = 0. \tag{4.3.19}$$

Using Eqs.(4.3.16)-(4.3.18), with the help of Eq.(4.3.19), we get

$$\overline{m}_+(\xi) = \frac{\sigma_0}{\sqrt{2\pi}(\epsilon + i\xi)}\left(\frac{K_+(\xi)}{K_+(i\epsilon)} - 1\right), \tag{4.3.20}$$

$$\overline{n}_-(\xi) = \frac{\sigma_0}{\sqrt{2\pi}(\epsilon + i\xi)K_+(i\epsilon)K_-(\xi)}. \tag{4.3.21}$$

For constant loading we may take $\epsilon \to 0$. Thus the above relations become

$$\overline{m}_+(\xi) = \frac{\sigma_0}{\sqrt{2\pi}(i\xi)}\left(\frac{K_+(\xi)}{K_+(0)} - 1\right), \tag{4.3.22}$$

$$\overline{n}_-(\xi) = \frac{\sigma_0}{\sqrt{2\pi}(i\xi)K_+(0)K_-(\xi)}. \tag{4.3.23}$$

In order to determine the analytical expression of SIF without factorizing the kernel $K(\xi)$, the method given by Nilsson [114, 115] is used. Here, the asymptotic expression of SIF can be found by knowing the values of the kernel for large and small values of ξ. Hence the asymptotic values for kernel $K(\xi)$ are given as

$$\lim_{\xi\to\infty}\frac{K(\xi)}{\xi}=\frac{-C_{44}^{(1)}G^{(1)}C_{44}^{(2)}G^{(2)}}{(C_{44}^{(1)}G^{(1)}+C_{44}^{(2)}G^{(2)})}=l_1, \tag{4.3.24}$$

$$\lim_{\xi\to 0}K(\xi)=\frac{-C_{44}^{(1)}C_{44}^{(2)}}{h(C_{44}^{(1)}+C_{44}^{(2)})}=l_2. \tag{4.3.25}$$

For a large value of ξ, the Eqs.(4.3.22) and (4.3.23) can be rewritten as

$$\lim_{\xi\to\infty}\overline{m}_+(\xi)=\lim_{\xi\to\infty}\frac{\sigma_0}{\sqrt{2\pi}(i\xi)}\left(\frac{K_+(\xi)}{K_+(0)}\right), \tag{4.3.26}$$

$$\lim_{\xi\to\infty}\overline{n}_-(\xi)=\lim_{\xi\to\infty}\frac{\sigma_0}{\sqrt{2\pi}(i\xi)K_+(0)K_-(\xi)}. \tag{4.3.27}$$

Asymptotic expressions of the above expressions using Eqs.(4.3.24) and (4.3.25) obtained as

$$\overline{m}_+(\xi)=\frac{\sigma_0\sqrt{l_1}}{\sqrt{2\pi l_2}i\,(-1)^{1/4}}\xi^{-1/2}, as\ \ \xi\to\infty, \tag{4.3.28}$$

$$\overline{n}_-(\xi)=\frac{\sigma_0}{\sqrt{2\pi l_1 l_2}i\,(-1)^{1/4}}\xi^{-3/2}, as\ \ \xi\to\infty. \tag{4.3.29}$$

The inverse fourier transform of the above functions can be determined as

$$\lim_{x\to 0^+}m(x)=\frac{-\sigma_0}{2}\sqrt{\frac{l_1}{\pi l_2}}x^{-1/2}, \tag{4.3.30}$$

$$\lim_{x\to 0^-}n(x)=-\sigma_0\sqrt{\frac{1}{\pi l_1 l_2}}(-x)^{1/2}. \tag{4.3.31}$$

Here the Eq.(4.3.30) represents shear component distribution on the outside of the crack along $x-$axis. Also, this shows the square root singularity at the origin i.e., the crack tip, which is very much expected through the nature of the problem. The Eq.(4.3.31) represents the displacement component in the vicinity of the crack tip, which is useful to obtain the crack opening displacement.

4.4 Stress intensity factor(SIF) and Crack opening displacement(COD)

The stress intensity factor (K_{III}) for the model is obtained as

$$K_{III}=\lim_{x\to 0^+}\sqrt{2\pi x}\ \sigma_{yz}^{(1)}(x,0)=-\sigma_0\sqrt{\frac{l_1}{2l_2}} \tag{4.4.1}$$

After putting the value of σ_0 in the Eq.(4.4.1), the value of SIF for the original problem(normalized with respect to $w_0^{(1)}$) becomes

$$SIF = \frac{C_{44}^{(1)}}{h}\sqrt{\frac{l_1}{2l_2}}. \tag{4.4.2}$$

The Crack Opening Displacement (COD) is obtained as

$$COD = -2\sigma_0\sqrt{\frac{1}{\pi l_1 l_2}}\sqrt{-x} \tag{4.4.3}$$

After putting the value of σ_0 in the Eq.(4.4.3), we get the expression of COD for the original problem(normalized with respect to $w_0^{(1)}$)given as

$$COD = \frac{2C_{44}^{(1)}}{h}\sqrt{\frac{1}{\pi l_1 l_2}}\sqrt{-x}. \tag{4.4.4}$$

4.5 Numerical results and discussion

For numerical calculation, three different composite materials and their combinations as Medium-I and Medium-II have been used, whose Engineering material elasticity constants (in GPA unit) are given in Table 4.1.

Composite Materials	C_{44}	C_{55}	ρ
Graphite epoxy	5.40	5.50	1.60
Carbon Fiber	6.15	6.15	1.5
Prepreg	7.8	7.8	1.595

Table 4.1: Engineering material elasticity constants

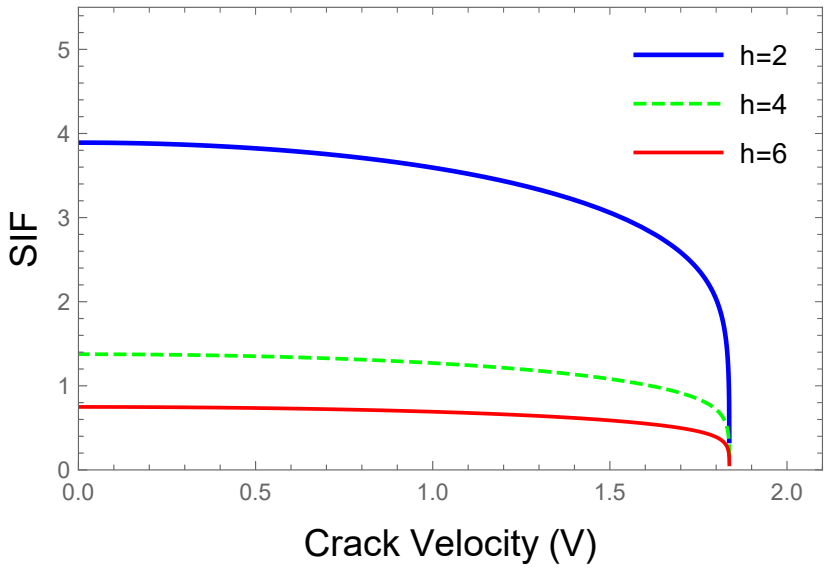

Figure 4.3: Variations of the normalized SIF vs Crack Velocity (V) for $h = 2, 4$ and 6 for Graphite epoxy as Medium-I and Carbon fiber as Medium-II.

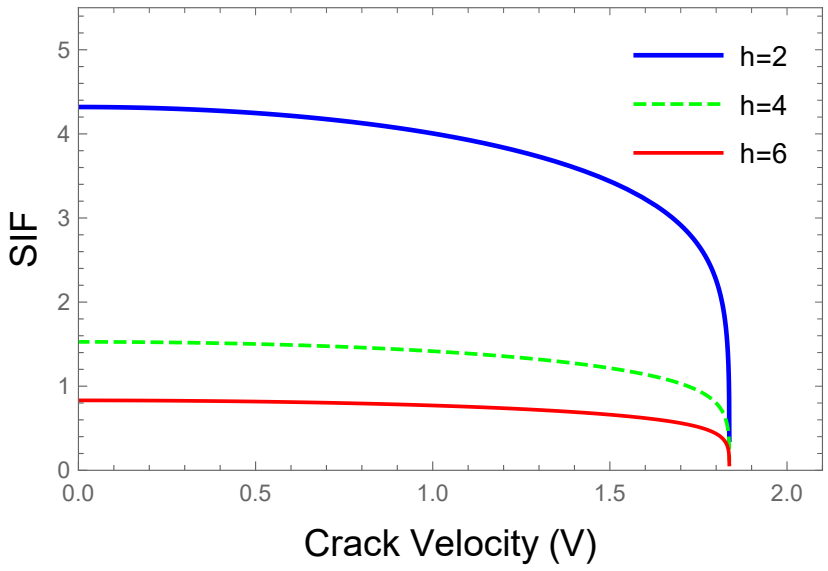

Figure 4.4: Variations of the normalized SIF vs Crack Velocity (V) for $h = 2, 4$ and 6 for Graphite epoxy as Medium-I and Prepreg as Medium-II.

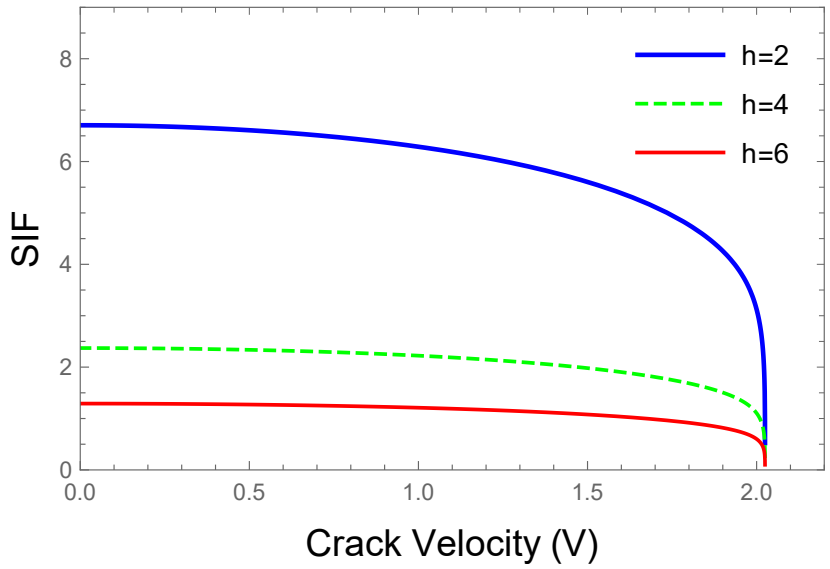

Figure 4.5: Variations of the normalized SIF vs Crack Velocity (V) for $h = 2, 4$ and 6 for Prepreg as Medium-I and Carbon fiber as Medium-II.

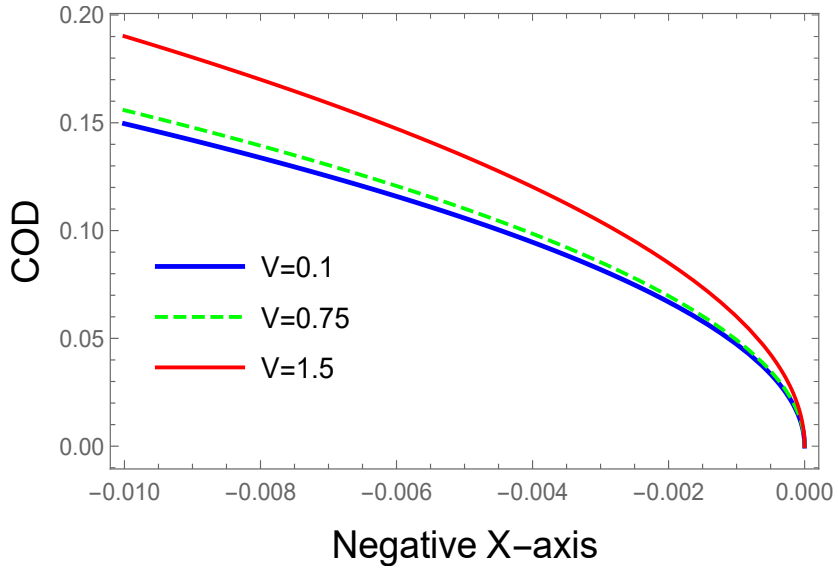

Figure 4.6: Variations of the normalized COD with distance x for Crack Velocity $(V) = 0.1, 0.75$ & 1.5 and $h = 2$ for Graphite epoxy as Medium-I and Carbon fiber as Medium-II.

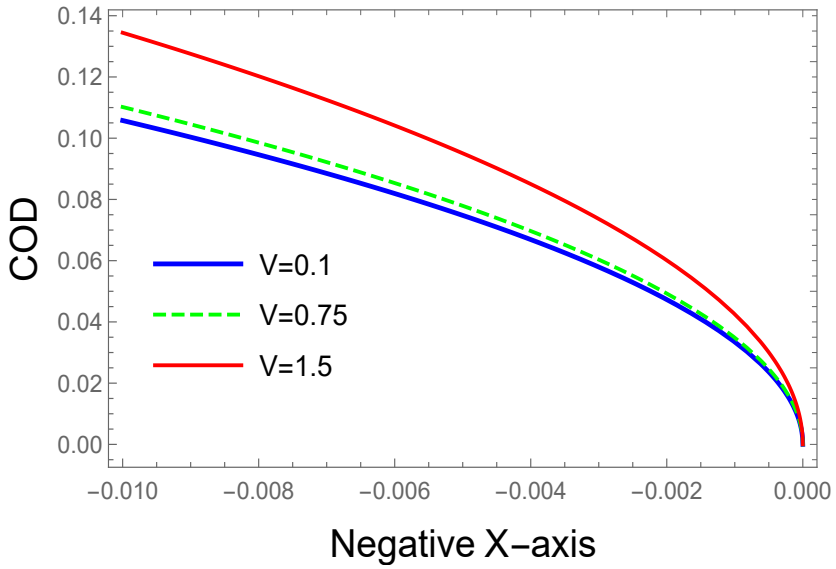

Figure 4.7: Variations of the normalized COD with distance x for Crack Velocity $(V) = 0.1, 0.75$ & 1.5 and $h = 4$ for Graphite epoxy as Medium-I and Carbon fiber as Medium-II.

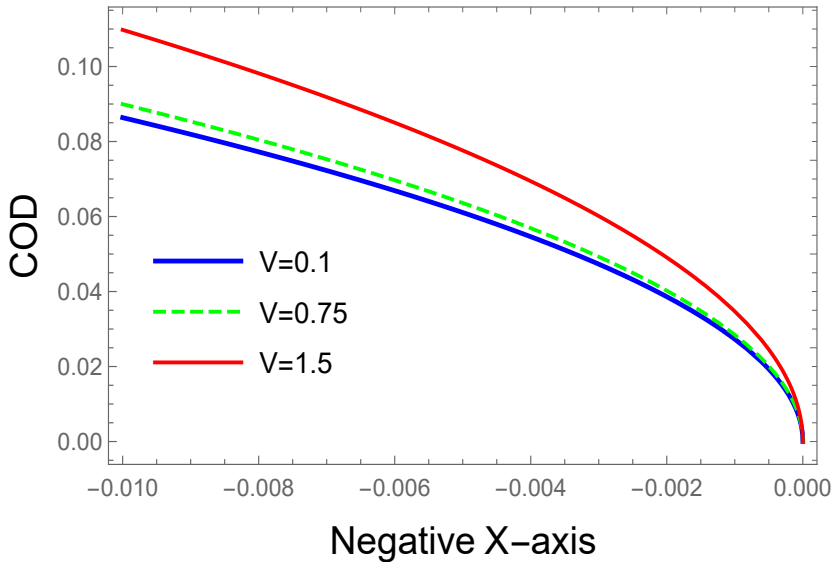

Figure 4.8: Variations of the normalized COD with distance x for Crack Velocity $(V) = 0.1, 0.75$ & 1.5 and $h = 6$ for Graphite epoxy as Medium-I and Carbon fiber as Medium-II.

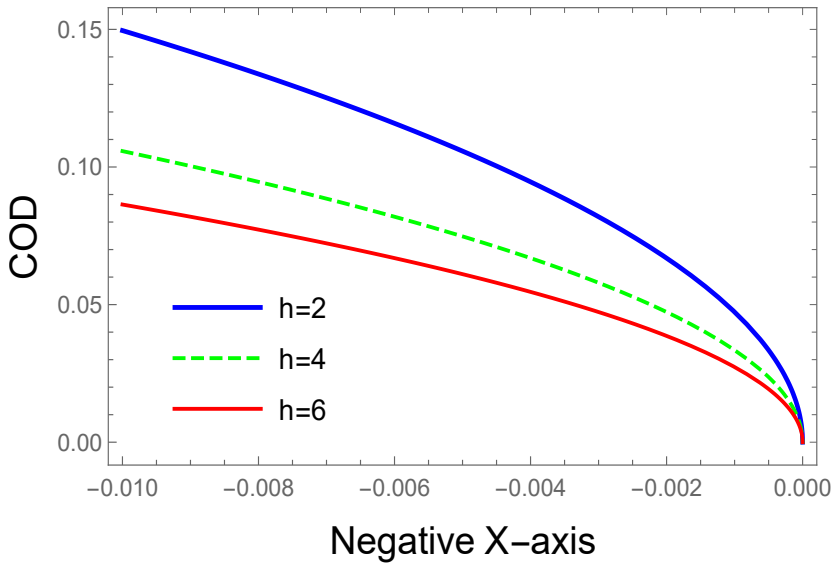

Figure 4.9: Variations of the normalized COD with distance x for Crack Velocity $(V) = 0.1$ and $h = 2, 4$ & 6 for Graphite epoxy as Medium-I and Carbon fiber as Medium-II.

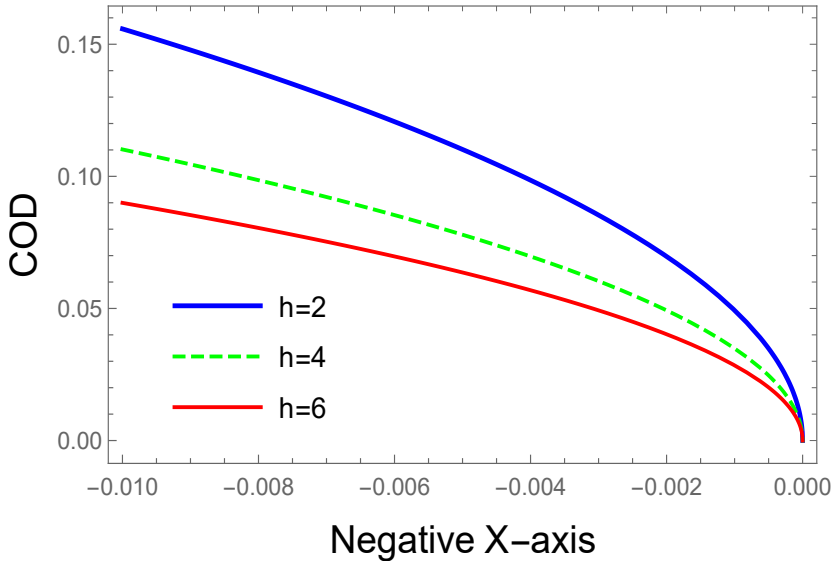

Figure 4.10: Variations of the normalized COD with distance x for Crack Velocity $(V) = 0.75$ and $h = 2, 4$ & 6 for Graphite epoxy as Medium-I and Carbon fiber as Medium-II.

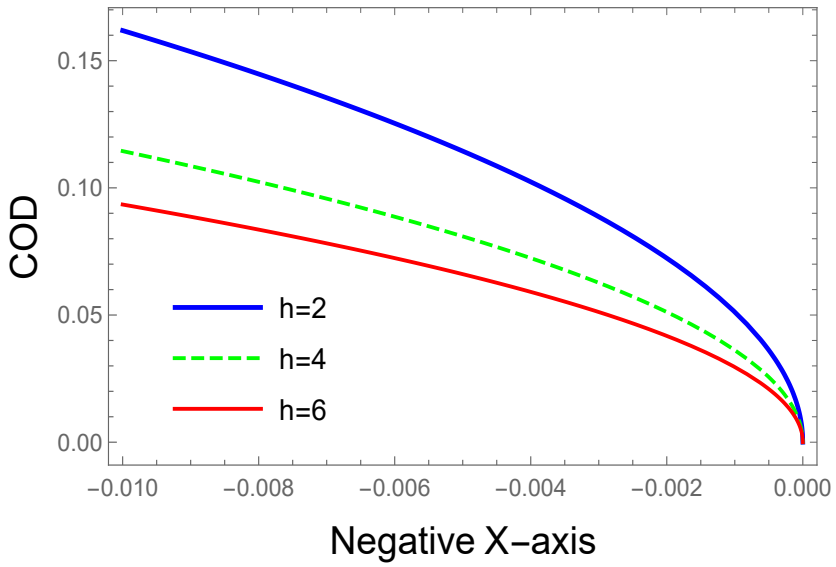

Figure 4.11: Variations of the normalized COD with distance x for Crack Velocity $(V) = 1$ and $h = 2, 4$ & 6 for Graphite epoxy as Medium-I and Carbon fiber as Medium-II.

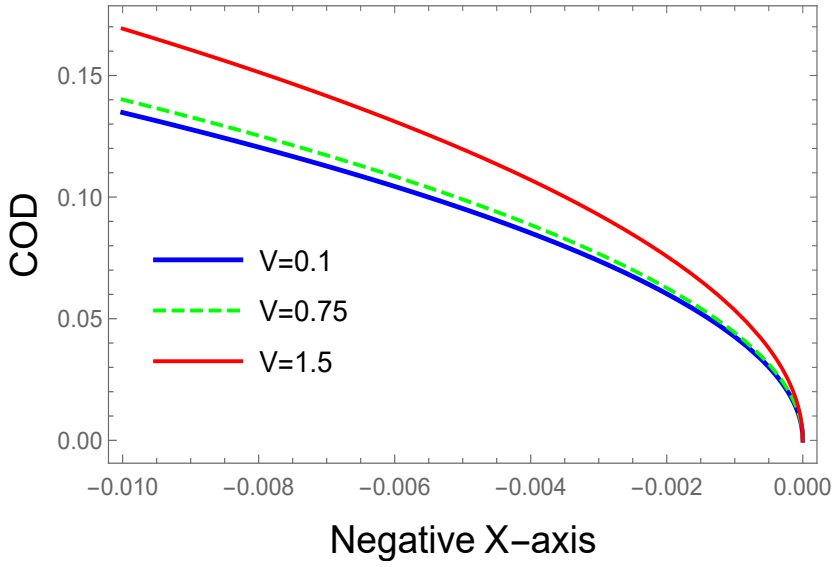

Figure 4.12: Variations of the normalized COD with distance x for Crack Velocity $(V) = 0.1, 0.75$ & 1.5 and $h = 2$ for Graphite epoxy as Medium-I and Prepreg as Medium-II.

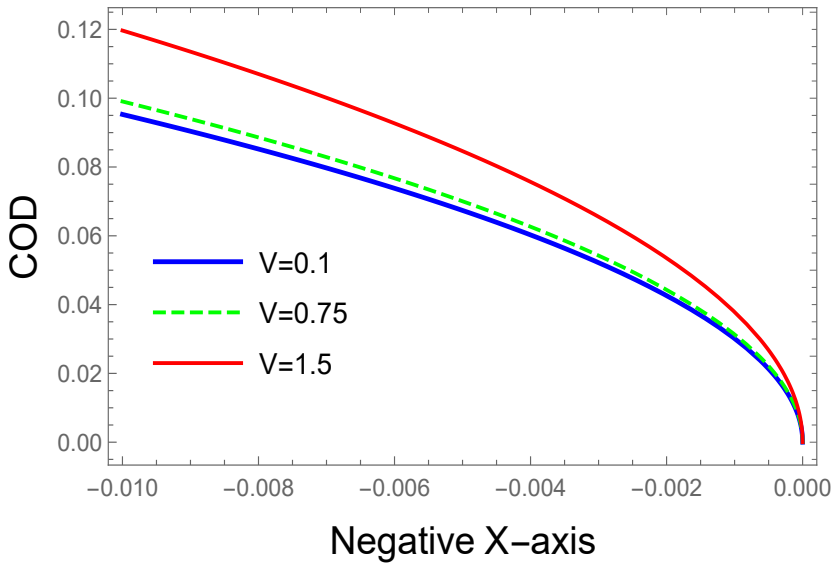

Figure 4.13: Variations of the normalized COD with distance x for Crack Velocity $(V) = 0.1, 0.75$ & 1.5 and $h = 4$ for Graphite epoxy as Medium-I and Prepreg as Medium-II.

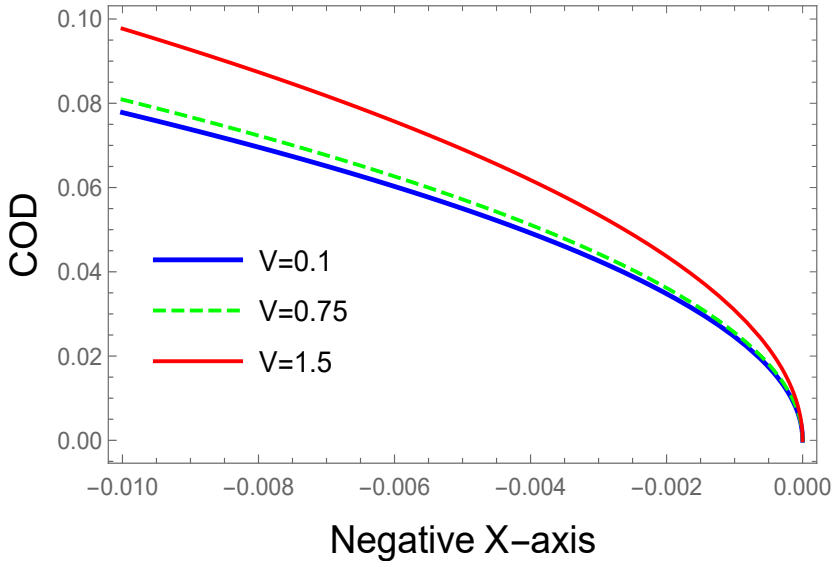

Figure 4.14: Variations of the normalized COD with distance x for Crack Velocity $(V) = 0.1, 0.75$ & 1.5 and $h = 6$ for Graphite epoxy as Medium-I and Prepreg as Medium-II.

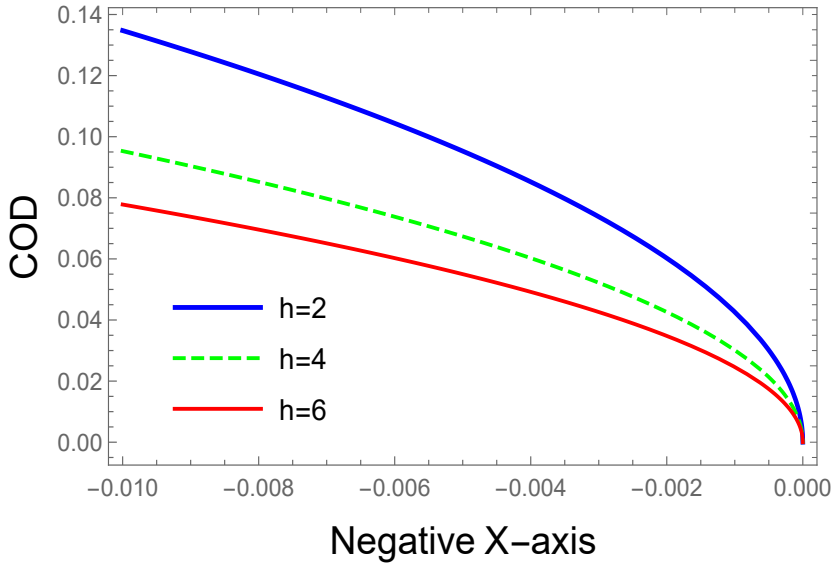

Figure 4.15: Variations of the normalized COD with distance x for Crack Velocity $(V) = 0.1$ and $h = 2, 4$ & 6 for Graphite epoxy as Medium-I and Prepreg as Medium-II.

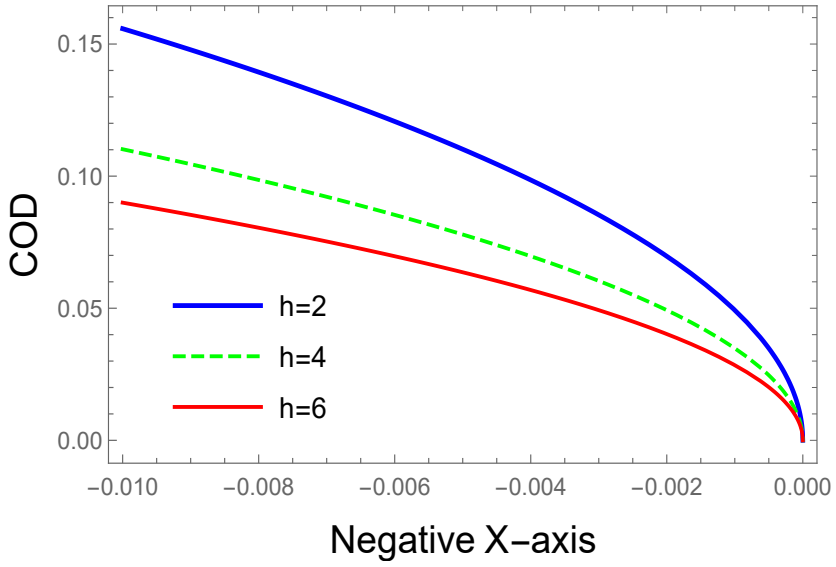

Figure 4.16: Variations of the normalized COD with distance x for Crack Velocity $(V) = 0.75$ and $h = 2, 4$ & 6 for Graphite epoxy as Medium-I and Prepreg as Medium-II.

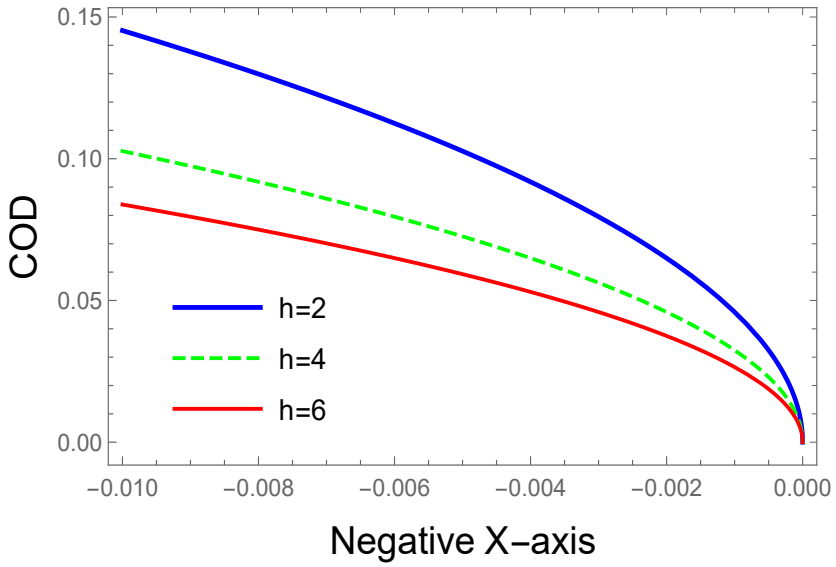

Figure 4.17: Variations of the normalized COD with distance x for Crack Velocity $(V) = 1$ and $h = 2, 4$ & 6 for Graphite epoxy as Medium-I and Prepreg as Medium-II.

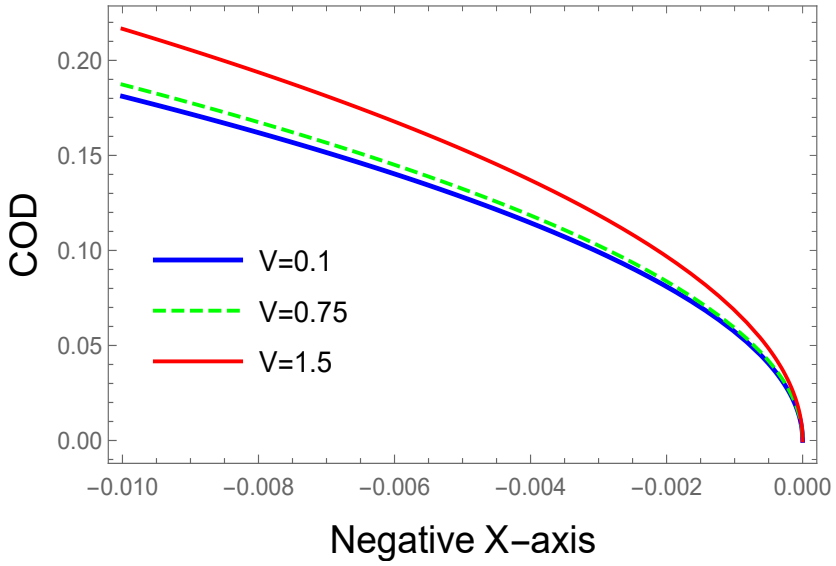

Figure 4.18: Variations of the normalized COD with distance x for Crack Velocity $(V) = 0.1, 0.75$ & 1.5 and $h = 2$ for Prepreg as Medium-I and Carbon fiber as Medium-II.

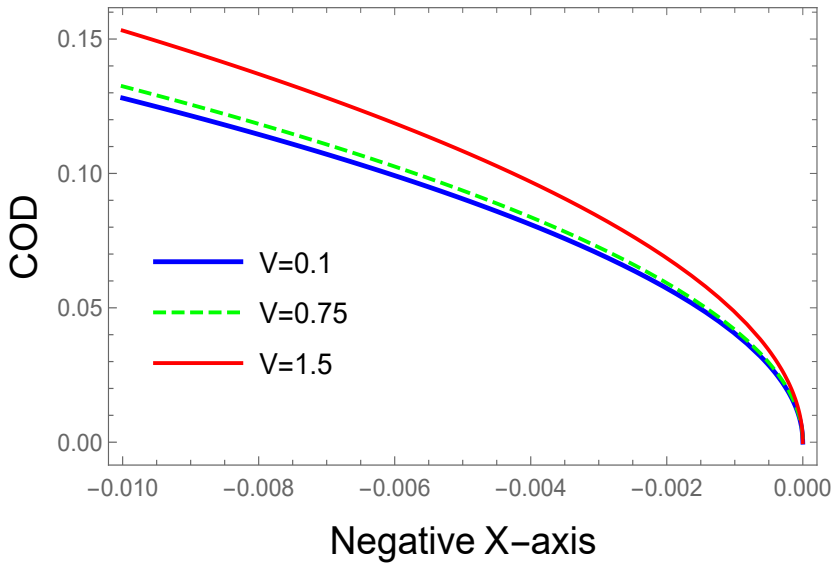

Figure 4.19: Variations of the normalized COD with distance x for Crack Velocity $(V) = 0.1, 0.75$ & 1.5 and $h = 4$ for Prepreg as Medium-I and Carbon fiber as Medium-II.

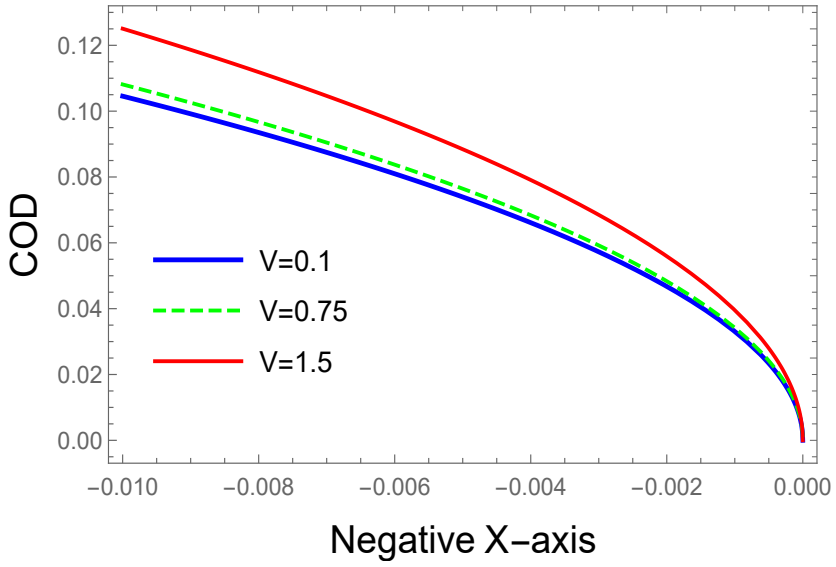

Figure 4.20: Variations of the normalized COD with distance x for Crack Velocity $(V) = 0.1, 0.75$ & 1.5 and $h = 6$ for Prepreg as Medium-I and Carbon fiber as Medium-II.

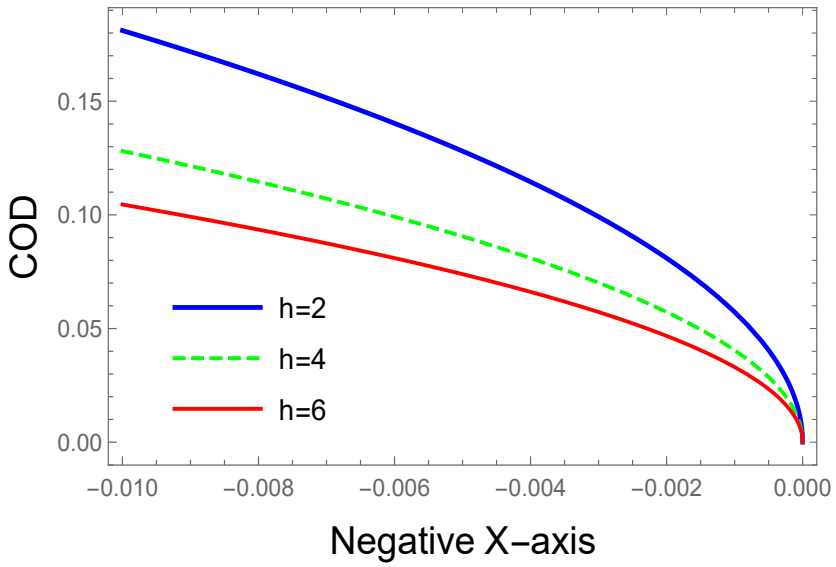

Figure 4.21: Variations of the normalized COD with distance x for Crack Velocity $(V) = 0.1$ and $h = 2, 4$ & 6 for Prepreg as Medium-I and Carbon fiber as Medium-II.

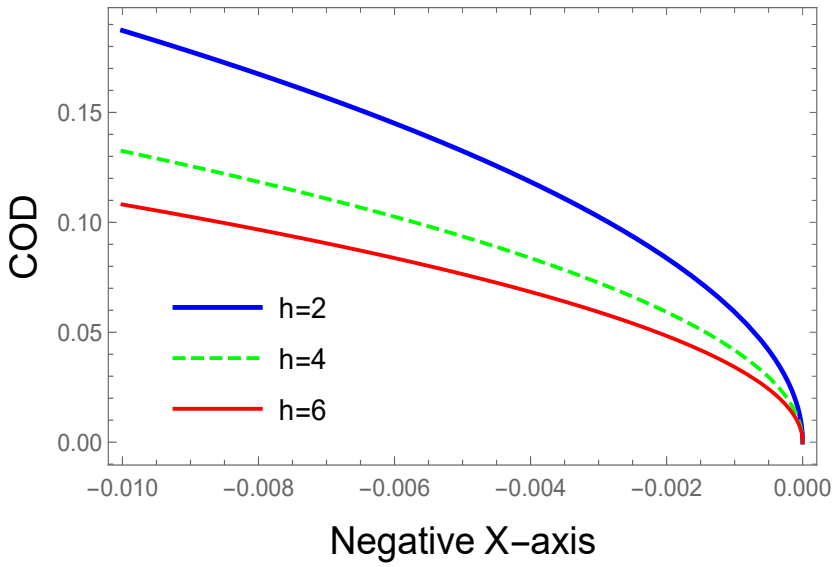

Figure 4.22: Variations of the normalized COD with distance x for Crack Velocity $(V) = 0.75$ and $h = 2, 4$ & 6 for Prepreg as Medium-I and Carbon fiber as Medium-II.

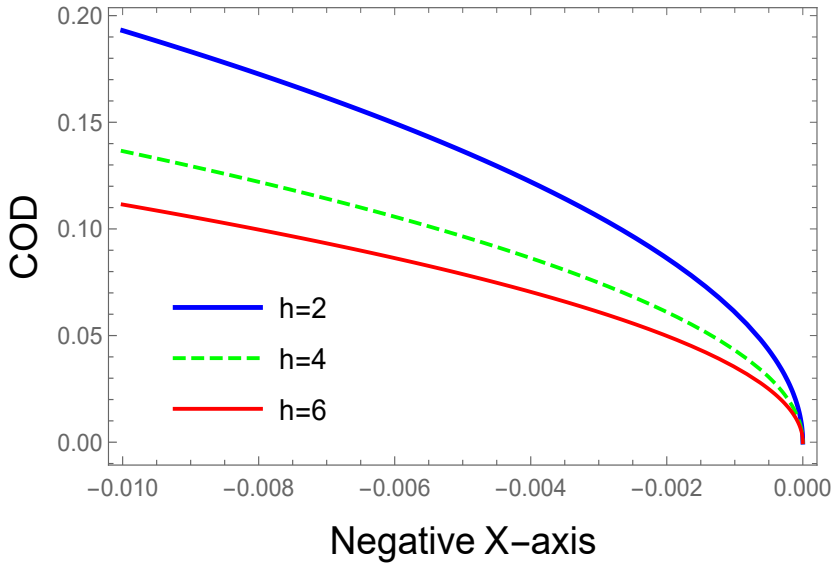

Figure 4.23: Variations of the normalized COD with distance x for Crack Velocity $(V) = 1$ and $h = 2, 4$ & 6 for Prepreg as Medium-I and Carbon fiber as Medium-II.

The analytical expressions of SIF and COD from the Eqs. (4.4.2) and (4.4.4) are seen to be depending on material constants and crack velocity. SIF is dependent on depth of the strip and the material properties. The effects of depth of the strip vs. crack velocity have been shown in Figs. 4.3-4.5. It is observed that the upper limit of crack velocity (V) is the SH-wave velocity (C_s), therefore for the mode-III crack propagation, crack velocity is always less than SH-wave velocity and SIF tends to zero as $V \to C_s$. The value of SIF is higher for the combination of materials, Graphite-epoxy as medium-I and Preprag as medium-II. Also in each combination of materials, it is observed that as the depth of the strip increases, the SIF decreases. Hence, the SIF can be controlled by increasing the depths of the strips to prevent material failure.

The variations of COD are found from Figs. 4.6-4.8 for Graphite epoxy as medium-I and Carbon fiber as medium-II. It is seen that the values of COD increase with the increase of crack velocity and it approaches to zero as the crack tip approaches to the origin, which justifies the physical nature of the problem. From Figs. 4.9-4.11, the effects of depth on the COD are seen as the depth increases the values of COD decreases. Although the values of COD are quiet similar for all the combinations of materials but the values of COD are slightly higher for the combination of materials: Graphite-epoxy as medium-I and Preprag as medium-II. Hence, The COD can also been controlled by increasing the depth of the strip and it tends to be zero as the crack tip reaches the origin. Similar behavior of SIF and COD have been observed through Figs. 4.12-4.23 for other combinations of composite materials

viz., Graphite epoxy as medium-I and Prepreg as medium-II, and also for Prepreg as medium-I and Carbon fiber as medium-II.

4.6 Conclusion

This chapter has studied the semi-infinite moving crack situated at the interface of dissimilar orthotropic strips. The chapter has achieved three important goals:

1. Converting the mixed boundary value problem to the Wiener-Hopf equation using Fourier transformation to determine the asymptotic expression for SIF at the crack tip.

2. Finding the asymptotic expression of COD analytically using the Wiener-Hopf technique.

3. The graphical presentations of the physical quantities like SIF and COD for various crack velocities and depths of the strips.

For various combinations of orthotropic materials, the characteristics of the model for crack propagation and crack opening displacement have been graphically shown. By altering the parametric values, which include the material constants and the depths of the strips, SIF and COD may be controlled, and the structure may be maintained by arresting the crack. The chapter might be helpful for the researchers and scientists to use the model that has been developed to improve laminate construction and forecast crack arrest when applying appropriate loadings and orthotropic materials.